Journal of Materials Chemistry A

Accepted Manuscript

ROYAL SOCIETY OF CHEMISTRY

www.rsc.org/materialsA

Cite this: DOI: 10.1039/c0xx00000x

www.rsc.org/xxxxxx

ARTICLE TYPE

Mechanism for improving the cycle performance of $LiNi_{0.5}Mn_{1.5}O_4$ by RuO_2 surface modification and increasing discharge cut-off potentials

Da Hong,[a] Yufeng Guo,[b] Huixin Wang,[a] Jigang Zhou[c] and Hai-Tao Fang*[a]

Received (in XXX, XXX) Xth XXXXXXXXX 20XX, Accepted Xth XXXXXXXXX 20XX

DOI: 10.1039/b000000x

The cycle performance of $LiNi_{0.5}Mn_{1.5}O_4$ (LNMO) is improved greatly by a surface modification with discrete RuO_2 particles in combination with setting discharge cut-off potentials to 4.5 V. A specific capacity value as high as 113.8 mAh/g after 1000 cycles is attained. In order to not only clarify the mechanism for the improvement by the RuO_2 particles deposited, but also elucidate which chemical property of surface-modifying materials play a critical role in the evolution of solid electrolyte interphase (SEI) layer with cycling, the electrochemical impedance spectra and X-ray photoelectron spectra (XPS) of bare LNMO electrode, discrete RuO_2 particles modified-LNMO electrode and discrete Al_2O_3 particles modified-LNMO electrode were compared. The XPS spectra of the SEI layers of these electrodes cycled between 4.5-5.2 V indicates that a stable SEI layer on the RuO_2-modified LNMO electrode has the characteristic of relatively higher content of LiF and longer poly-ethylenecarbonate chains with extremely low content of -CF_2O- groups. The crucial point for the formation of the stable SEI layer is the sustainable consumption of the F radicals generated by the electrochemical decomposition of $LiPF_6$ at high potentials. We conclude that the hydrolysable property of ruthenium fluorides, intermediate products during the formation of SEI layer on the RuO_2-modified LNMO electrode, and the high catalytic activity of RuO_2 itself for electrochemical oxygen evolution guarantee the sustainable consumption of the F radicals. Al_2O_3 is lack of these special chemical properties to attain the sustainable consumption, thus leading to no improvement by the modification with discrete Al_2O_3 particles.

Introduction

Under demand by electrical vehicles, hybrid electrical vehicles and plug-in hybrid electric vehicles, obtaining high energy density is an everlasting aim for studying Li-ion batteries.[1] The high energy density can be achieved by enhancing either voltage or specific capacity. $LiNi_{0.5}Mn_{1.5}O_4$ (denoted as LNMO) is considered as one of the most promising high energy density cathode materials for Li-ion batteries because of its higher potential plateau of 4.7 V (vs Li^+/Li) and its theoretical specific capacity of 146.7 mAh/g comparable with conventional $LiCoO_2$ and $LiFePO_4$ cathode materials.[2, 3] The theoretical energy density of LNMO/graphite lithium ion battery (LIB) is 650 Wh/kg, 20% and 30% more than conventional $LiCoO_2$/graphite LIB and $LiFePO_4$/graphite LIB, respectively.[4, 5]

However, it is well known that the cycle performance of LNMO is far from satisfactory to meet real applications. Two respects are usually considered to attribute to its capacity fading with cycling. One is the corrosion of LNMO by the HF, which is formed by the decomposition of electrolytes at high potentials.[6-8] The other one is the deterioration of solid electrolyte interphase (SEI) layer on LNMO electrodes with cycling, such as thickening or accumulating fluorides, which greatly hinders the diffusion of Li^+ through the SEI layer.[9, 10] As a consequence, the impedance and polarization of LNMO electrodes are increased with cycling then deteriorating the cycle performance.[11, 12]

The surface modification of LNMO is considered to be an effective strategy to improve the cycle performance. The first attempt was conducted by Sun and coworkers, [8] who coated ZnO on the surface of LNMO and found the cycle performance is improved greatly. They ascribed the improvement to the consumption of HF in the electrolyte by chemical reaction with the ZnO and the protection of LNMO from the HF corrosion. Wu et al reported, in the case of ZrO_2-modified LNMO, only a complete ZrO_2 coating can improve the cyclic performance, while an incomplete ZrO_2 coating brings a negligible enhancement.[13] This result seems supporting the viewpoint mentioned by Sun. Arrebola and his coworkers restudied ZnO-modified LNMO. They found that a surface modification by discrete ZnO particles, a case of incomplete coating, can improve cyclic performance as well.[14] But following the explanation by Sun, they also considered that the reason for the improvement is the consumption of HF by ZnO. Besides ZnO, SiO_2 and BiOF coated are all considered as HF scavengers and protective layers at the same time to alleviate the HF corrosion.[6, 11, 15] However, it needs to be noted that one product of reactions between metal oxides coated and HF is H_2O, which can react with the electrolytes of LIBs to repeatedly generate HF.[16, 17] This reaction together with the improvement of LNMO cycle performance by the surface

modification with discrete ZnO particles, indicates that the explanation for improving the cycle performance based only on the HF corrosion does not make sense for all cases of LNMO surface modifications. The mechanism for the cycle-performance improvement of LNMO by various surface modifications needs to be further recognized.

The effect of the SEI layer on the performance of cathode materials has drawn intensive attention since Goodenough has suggested that a SEI layer also exists between a cathode and electrolyte as graphite anodes.[18, 19] He also stated that the greatest challenge for high-potential electrode materials is how to obtain a stable SEI layer.[20] Manthiram and coworkers investigated surface modifications of LNMO using several materials including Al_2O_3, ZnO, Bi_2O_3 and $AlPO_4$.[12, 21] Their explanation for the improvement by surface modifications is that the coating materials can slow down the growth of SEI layer by suppressing side reactions between electrolytes and LNMO electrode. Discussions in several studies involving different coating materials, such as $AlPO_4$, AlF_3, Bi_2O_3, LiPON, carbon and graphene oxide,[10, 22-26] support the explanation based on the evolution of SEI impedance. Besides restraining the increase of SEI impedance with cycling, it is reported by Aurbach that the composition of SEI layer can be changed slightly by MgO or ZnO surface modifications.[12] Veith compared LNMO electrodes modified by Al_2O_3, ZnO and ZrO_2, respectively.[27] His results indicate that the formation and evolution of SEI layer is dependent on coating materials. However, in-depth analyses on the mechanism for following important aspects are still very scarce. Firstly, how a suitable modifying material favours the formation of SEI layer with stable impedance? Secondly, what is the inherent relation between the chemical properties of modifying materials and the composition characteristics of different SEI layers? Undoubtedly, it is of scientific importance to answer these two questions.

RuO_2 is a special metal oxide with its unique high electronic conductivity and catalytic functions for many electrochemical oxidation processes, such as electrochemical oxygen evolution reaction.[28] The rate capabilities of $LiFePO_4$ and TiO_2 electrodes can be improved greatly by an incorporation of RuO_2.[29, 30] Liu reported that the cycle performance of $Li_{1.2}Mn_{0.54}Ni_{0.13}Co_{0.13}O_2$ electrode was deteriorated by the RuO_2 coating.[31] Nevertheless, this result does not definitely mean that a surface modification by RuO_2 will definitely degrade the performance of LNMO. Here, we demonstrate that the cycle performance of LNMO is improved evidently by the surface modification with discrete RuO_2 particles in combination with increasing discharge cut-off potentials. The effect of discharge cut-off potentials on the cyclic performance of bare LNMO and the RuO_2 modified LNMO is discussed in advance. Thereafter, in order to not only clarify the mechanism for the improvement by RuO_2 coated, but also elucidate which chemical property of coating materials play a critical role in the evolution of SEI with cycling, a comparison between two surface modifications by discrete Al_2O_3 particles and by discrete RuO_2 particles, respectively, is presented.

Experimental

Material synthesis

The LNMO spinel powder used was purchased from Hunan Shanshan Corp., China. The surface modification with RuO_2 is attained by mixing LNMO (6.32g) and NaOH (0.3 M, 50 mL) solution first, then pouring the mixture into a $RuCl_3$ solution (0.1 M, 25 mL) and stirring until precipitated completely. The precipitate was washed with deionized water to remove the residual Na^+ and Cl^-, then dried at 60 °C in an oven, and finally annealed at 400 °C for 19 h in the air. The amount of RuO_2 in the composite was designed to be 5 wt%. The RuO_2-modifed LNMO prepared with the NaOH solution is denoted as RuO_2-LNMO.

A sol-gel process was used to deposit Al_2O_3 on the surface of LNMO particles. The LNMO powder (5 g) was firstly added into an aluminium isopropoxide ethanol solution (0.1 M, 50 mL). After adding 270 μL H_2O, the solution was stirred for 3 h to make the aluminium isopropoxide hydrolyzed completely. The precipitate was washed with ethanol for 3 times, then filtered and dried at 50 °C overnight, and finally calcined at 700 °C for 3 h. The amount of Al_2O_3 in the composite was also designed to be 5 wt%. The Al_2O_3-modifed LNMO is denoted as Al_2O_3-LNMO.

Materials Characterization

X-ray diffraction (XRD) spectra were obtained using D-MAX/2400 diffractometer with Cu Kα radiation. Scanning electron microscope (SEM) observation, energy diffraction spectrum (EDS) analysis and elemental mapping characterization were performed using FEI Nova Nano 430 system or FEI 200FEG, both equipped with an Energy Dispersive XRay spectrometer. X-ray photoelectron spectra (XPS) were collected using a Thermofisher Scienticfic K-Alpha spectroscopy equipped with a monochromatic Al-Kα X-ray source to analyze the chemical state of elements in the SEI layers of cycled LNMO electrodes. All XPS spectra were calibrated with the peak of Pt $4f_{7/2}$ spectrum at 71.0 eV. To prepare the cycled LNMO electrodes, all the coin cells were disassembled and then washed three times by Dimethyl carbonate (DMC) in a glove box. All LNMO electrodes were sealed up in the glove box after their preparations and transferred to the test chamber immediately before conducting XPS. All cycled lithium anodes were directly analyzed without washing to detect Mn ions dissolved in the electrolyte and metallic Mn deposited on lithium anodes as much as possible.

Electrochemical Measurements

Cathodes were prepared by casting a slurry of the LNMO or surface-modified LNMO, super P (Timcal), and polyvinylidene fluoride (PVDF, Alfa Aeser) in an *N* -methyl pyrrolidone (NMP, Alfa Aeser) onto an aluminium foil. The weight ratio of LNMO: super P: PVDF is 8:1:1. The loading amount of active materials is 2.0-2.3 mg/cm^2 in area density and 15±2 um in thickness. The CR2032 coin cells were assembled in argon-filled glove-box with the fabricated cathodes, lithium foil anodes, an electrolyte of 1 M $LiPF_6$ in ethylene carbonate/dimethyl carbonate (EC/DMC,

Novolyte Tech, Suzhou), and Celgard M824 separators. All the cells were cycled with 1 C rate (146.7 mA/g) at 25 °C except the first three cycles with 0.2 C rate for cells cycled with the discharge cut-off voltage of 4.5 V. All capacity values in this paper are based on the mass of LNMO. The electrochemical impedance spectra (EIS) were obtained using a potentiostat (Autolab PGSTAT302N) equipped with a frequency response analyzer. All EIS data were collected after resting LNMO electrodes at open circuit potentials of 50% state of charge for 1 h.

Results and discussion

Morphology and structure characterization

The SEM morphologies of the bare LNMO, RuO_2-LNMO and Al_2O_3-LNMO are compared in Fig. 1. In low magnification, obvious change after the RuO_2 or Al_2O_3 modification is not present. The bare LNMO with particles size of about 10 μm has faceted shapes with smooth surface. The RuO_2-modified LNMO has small discrete RuO_2 particles with size of about 100 nm dispersed on the surface. Each particle of these two modified LNMOs is not fully coated as shown in Fig. 1d-f. The EDS element maps of RuO_2-LNMO and Al_2O_3-LNMO (Fig. S1) show the presence of some micron-sized RuO_2 or Al_2O_3 aggregates marked by arrows.

The X-ray diffraction (XRD) patterns of the bare LNMO, RuO_2-LNMO and Al_2O_3-LNMO (Fig. S2) indicate the LNMO used here contains ordered phase (P432 space group).[32, 33] On the other hand, the charge-discharge curves of the bare LNMO and RuO_2-LNMO with discharge cut-off potential of 3.0 V display a small plateau around 4 V, as shown in Fig. S3. This plateau corresponds to Mn^{3+}/Mn^{4+} redox process, which is a typical feature of disordered LNMO (group Fd32).[33, 34] Therefore, the LNMO spinel used here is a mixture of ordered and disordered phase.[35] The deposited RuO_2 or Al_2O_3 does not change the diffraction peaks of the LNMO, suggesting that Ru or Al does not diffuse into the lattice of LNMO after processes for the modifications.

Cycle-performance comparison

Fig. 2a compares the cycle performances of bare LNMO, RuO_2-modified LNMO (prepared with the NaOH solution) and Al_2O_3-modified LNMO electrodes with discharge cut-off potentials of 3.0 or 4.5 V, denoted as bare-3.0V, bare-4.5V, RuO_2-3.0V, RuO_2-4.5V and Al_2O_3-4.5V, respectively. The specific capacity of the bare-3V reaches 130.6 mAh/g at the ninth cycle, and fade rapidly to 18.0 mAh/g after 1000 cycles, only 13.8% of the its maximum specific capacity. When the discharge cut-off potential was raised to 4.5V, the bare LNMO electrode (bare-4.5V) has 59 mAh/g at 1000th cycle, retain 50.9% of its maximum capacity, much higher than the bare-3V. After modified by RuO_2, the cycle performance is improved further if discharge cut-off potential is set at 4.5 V, but completely not if set at 3.0 V. The RuO_2-4.5V delivers a discharge specific capacity of 77.3 mAh/g after 1000 cycles, up to 70.1% of its maximum capacity. Although the initial capacity of the RuO_2-4.5V is lowest, its capacity reaches highest after 270 cycles. The Al_2O_3 modification does not work as the RuO_2 modification. Actually, the Al_2O_3-4.5V has a close cycle performance with the bare-4.5V.

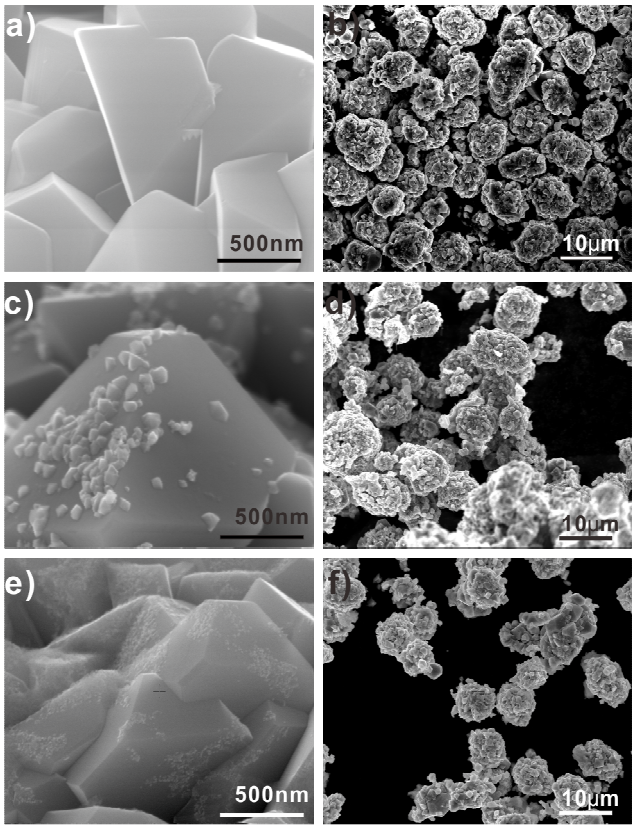

Fig. 1 SEM images of a, b) bare LNMO, c, d) RuO_2 modified LNMO, e, f) Al_2O_3 modified LNMO.

It is widely believed that more HF should be formed when the potentials are higher due to the electrochemical decomposition of $LiPF_6$.[12] Therefore, the improvement of the cycle performance by increasing discharge cut-off potential to 4.5 V and by the RuO_2 surface modification with discrete morphology unambiguously indicates that the capacity fading of LNMO with cycling cannot be simply ascribed to the HF corrosion.

Fig. 3c-g, the EDS of Li electrodes coupled with LNMO electrodes after 500 cycles, clearly show the presence of Mn element on black cycled Li electrodes if coresponding cut-off potentials are 3.0 V, but absence on grey cycled Li electrodes if coresponding cut-off potentials are 4.5V. The absence of Mn element is also proved by XPS analysis, as shown in Fig. S4. As any dissolved cations from LNMO cathodes can migrate to Li anodes under electronic field, and finally deposit on Li anodes with a very low potential, this comparison supports that the Mn dissolution is greatly suppressed by raising discharge cut-off potential to 4.5V. From the typical discharge curves of bare-3.0V and RuO_2-3.0V, as shown in Fig. S3a-b, discharges to 3.0 V always pass through the Mn^{3+}/Mn^{4+} plateau at 4.0 V, while discharges to 4.5 V not. Mn^{3+} ions involved in this redox reaction is from disordered phase of the LNMO used and they are prone to

occur a disproportionate reaction ($Mn^{3+}\rightarrow Mn^{2+}+Mn^{4+}$) as Mn^{3+} ions of $LiMn_2O_4$. The Mn^{2+} ions formed are easy to be dissolved into electrolyte and then leading to faster capacity degradation.[36-38] Since Mn^{3+} ions will be oxidized to Mn^{4+} ions during charge process after the plateau at 4 V, raising cut-off potential from 3.0 V to 4.5 V can suppress the Mn dissolution. Accordingly, the cycle performance of bare and RuO_2-modified LNMO electrodes is improved if the cells were cycled between 4.5-5.2 V. This result is consistent with what Weishan Li et al recently reported,[39] that is, the cycle stability of LNMO at 55 °C is significantly improved by raising the cut-off discharge potential from 3.5 V to 4.0 V. They attributed the improvement to less suffering from the Mn dissolution and Jahn-Teller effect. The Mn dissolution leads not only to the structural destruction in LNMO surface region but also to the deposition of Mn fluorides in the SEI layers of LNMO electrodes.[17] Besides, the Mn^{3+}/Mn^{4+} redox reaction accelerates the formation of SEI layer.[40] All these factors impede the charge transfer and Li^+ diffusion processes of LNMO electrodes, thus degrades their capacity.

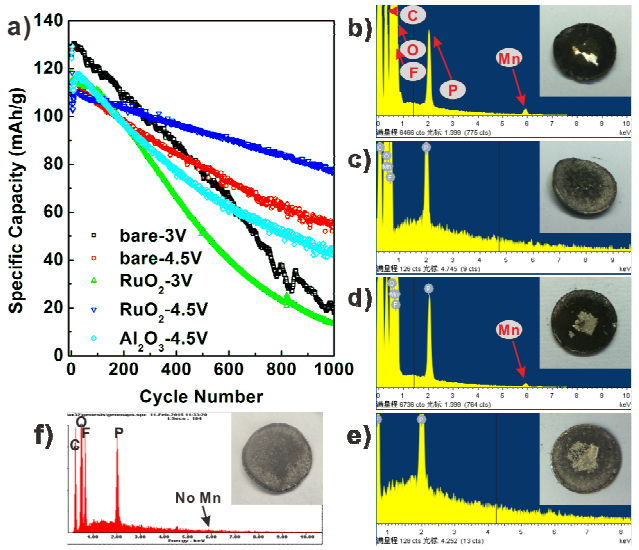

Fig. 2 a) cycle performances of the Bare-3V (black square), bare-4.5V (red circle), RuO_2-3V (green upper triangle), RuO_2-4.5V (blue lower triangle), Al_2O_3-4.5V (light blue diamond). EDS and optical photos of cycled Li electrodes coupled with b) Bare-3V, c) bare-4.5V, d) RuO_2-3V, e) RuO_2-4.5V, f) Al_2O_3-4.5V. Because of the attachment of all Li electrodes with separators, products deposited were peeled away at center parts of some Li electrodes when removed separators, resulting in lighter color. All EDS were collected from regions without peeling.

Why the surface modification by discrete RuO_2 particles can improve the cycle performance when setting discharge cut-off potential as high as 4.5V? In order to simplify this question, and more importantly, to clarify the inherent relation between intrinsic properties of modifying materials and the cycle performance, it is necessary to exclude the effect of the Mn dissolution and Mn^{3+}/Mn^{4+} redox reaction on the formation and composition of the SEI layer. Therefore, we focus on the bare-4.5V, RuO_2-4.5V and Al_2O_3-4.5V and compare their EIS and XPS results in following discussion.

EIS of the bare-4.5V, RuO_2-4.5V and Al_2O_3-4.5V

Fig 3a-c. display Nyquist plots of these three electrodes. Each plot consists of two arcs and a slope. Referring to previous study of 5 V spinel samples by Aurbach and Alcantara et al, the first arc at high-frequency region is ascribed to lithium-ion diffusion through the SEI layer.[41, 42] The second arc at medium to low frequency region is attributed to the charge transfer reaction. The slope at the low-frequency region is assigned to lithium-ion diffusion in the LNMO bulk. The radius of each arc is the resistance for the lithium-ion diffusion through the SEI layer and charge transfer reaction, called the resistance of SEI layer (R_{SEI}) and the resistance of charge transfer (R_{CT}). We measured the real-resistance spans (the Z' axis) of the high-frequency arcs as R_{SEI} values, and fitted a part of each Nyquist plot before the high-frequency arc by the Zview program to obtain R_{CT} values.

Fig. 3d-f show the variation trends of R_{SEI}, R_{CT} and their sum with cycling for the bare-4.5V, RuO_2-4.5V and Al_2O_3-4.5V. The R_{SEI} and R_{CT} of the bare-4.5V and Al_2O_3-4.5V all increase with cycling. While the R_{SEI} of the RuO_2-4.5V stays at about 20 Ohm, and its R_{CT} grows slightly, only 30 Ohm after 500 cycles. It is well known that the higher R_{SEI} and R_{CT}, the severer electrochemical polarization, leading to lower capacity. The variation trends of these three electrodes are consistent with their cycle performances, respectively. Fig. 3d clearly indicates that the RuO_2-4.5V has a stable SEI layer, but the bare-4.5V and Al_2O_3-4.5V not. To clarify the composition characteristics of the stable SEI layer, the XPS spectra of these three electrodes after 500 cycles and Ar ion sputtering for 30, 60, 90 and 120 s were compared.

XPS of the SEI layers

Fig. 4a-c displays F1s XPS spectra, which are fitted with peaks at 685.3, 687, 688 and 689.5 eV. Peaks at 685.3 eV and 688 eV are corresponding to LiF and PVDF, respectively. The peak at 687 eV can be assigned to $LiPF_6$, Li_xPOF_y and Li_xPF_y.[31, 43-45] Li_xPOF_y and Li_xPF_y are considered to be formed by the decomposition of $LiPF_6$ salt. The most evident difference among the F1s spectra is that the peak at ~689.5 eV is present in the spectra of the bare-4.5V and Al_2O_3-4.5V, while is very tiny, almost absent, in the spectra of the RuO_2-4.5 V. To the best of our knowledge, this peak has been detected on the MgO and ZnO modified LNMO electrodes after aged in an electrolyte (1.5M $LiPF_6$ in EC/DMC) at 60 °C by Aurbach et al.[46] They attributed this peak to C-F bond of $FCH_2CH_2OCO_2Li$, a possible product of nucleophilic attack of F radicals to the C-O bond in EC. However, the bonding energy of F1s in this compound should be lower than that of PVDF (688 eV). Ziv et al. suggested this peak is belong to $Li_xPF_yO_z$ due to the coexistence of high bonding energy O1s with P2p peak on cycled graphite anode at the same time.[47] However, as mentioned above, most researchers believe bonding energy of F1s in such compound should be close to $LiPF_6$.

O1s XPS of the cycled electrodes are shown in Fig. S5a-c. Peak at 531.5 eV refers to C=O and –OH, and peaks at ~532.5 and 533.5 eV are assigned to $ROCO_2Li$ and C-O, respectively.[27, 44, 48-50] Peak around 530 eV is from the metal-oxygen bonds of LNMO, RuO_2 and Al_2O_3. A tiny peak at 536 eV is present on the bare LNMO, while absent on the modified electrode. Because its appearance is synchronous with the F1s peak at 689.5 eV of the

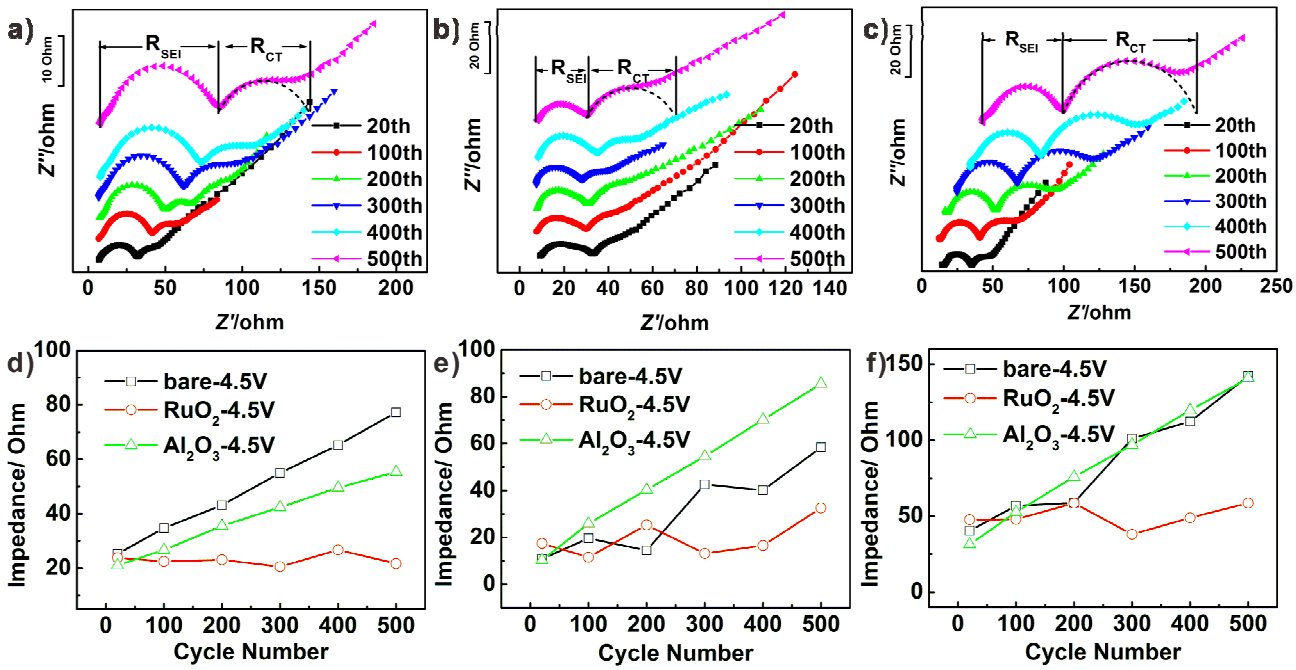

Fig. 3 Nyquist plots of a) bare-4.5 V, b) RuO_2 -4.5 V, c) Al_2O_3 -4.5 V. Variation of their d) R_{SEI}, e) R_{CT} and f) R_{SEI}+R_{CT} during cycling.

bare-4.5V, it is reasonable to believe that the F1s peak at 689.5 eV and O1s peak at 536 eV are from one same component in the SEI layer of the bare-4.5V. We consider that these two peaks should stand for a -CF_2O- functional group, because this group is the only way to synchronously obtain the F1s peak of such high bonding energy of 689.5 eV, even higher than that of F-C-F in PVDF, and the O1s peak as high as 536 eV by a mutual inductive effect between its F and C atoms.

Fig. 4d-e show the variation of two area ratios with the sputtering time for these three electrodes, the ratio of the F1s peak at 689.5 eV (-CF_2O-) and the ratio of F1s peak at 685 eV (LiF), respectively, with the sum of other F1s peaks except PVDF. Firstly, in the range of 30-90 s, the -CF_2O- ratio of the bare-4.5V is much higher than the others, and the Al_2O_3-4.5V has more -CF_2O- than the RuO_2-4.5V. The -CF_2O- ratios of three electrodes become close at 120 s. Secondly, except sputtering for 120 s, the RuO_2-4.5V shows highest content of LiF. Thirdly, the -CF_2O- ratio for the bare-4.5V drops sharply with sputtering, while change less for the Al_2O_3-4.5V and RuO_2-4.5V. Fourthly, the content of LiF changes less with sputtering for the RuO_2-4.5V, while increase evidently for the bare-4.5V and Al_2O_3-4.5V. These four points indicate that the stable SEI layer of the RuO_2-4.5V has extremely low content of -CF_2O- groups and relatively higher content of LiF, besides their contents change less with sputtering. It is not surprised to note that O1s peak at 536 eV is absent in the spectra of the RuO_2-4.5V and Al_2O_3-4.5V, since their F1s peaks at 689.5 eV are almost absent and weaker, respectively, and the content of O element is only half of F element in the -CF_2O- functional group.

In the following section, we will explain how the -CF_2O- functional group is formed and how the chemical properties of the coated materials, RuO_2 and Al_2O_3, affect the content of the -CF_2O- group and LiF. After that, the variation of the -CF_2O- and LiF content with sputtering for these three electrodes are further elucidated.

Mechanism for the dependence of the SEI-layer composition on the properties of RuO_2 and Al_2O_3

It has been reported that $LiPF_6$ is decomposed under high potentials by the reaction (1).[51]

$$PF_6^- - e^- \rightarrow PF_5 + F^{\bullet} \quad (1)$$

The ring of EC molecules can be opened due to the attack of F radicals and form monomers with a radical at one end, which are able to further attack another EC molecules and result in polymerization.[52] Based on which C-O bond of an EC molecule is broken, there are two ways for the polymerization as shown in Fig. 5a.[53] The product of the polymerization, poly-ethylenecarbonate (PEC), has the -CH_2O- group. F radicals, a kind of extremely strong Lewis acid, can substitute the H atoms of the -CH_2-O- group, leading to the formation of -CF_2O- groups in the PEC chains.

It is proper to think that the more F radicals react with the -CH_2-O- group, the higher the ratio of -CF_2O- is. Therefore, Fig. 4d indicates the amount of F radicals precipitating the formation of the PEC is lowest for the RuO_2-4.5V but highest for the bare-4.5V. Based on this point, we speculate the F radicals are consumed by the RuO_2 deposited by the reaction (2). It is reasonable to deduce that oxygen ions of RuO_2 can be oxidized by F radicals due to their extremely high oxidizability. Ruthenium fluorides can be hydrolyzed by water impurity in the

EC/DMC electrolyte,[54] resulting in the recovery of RuO_2 and the formation of HF by the (3-4) reactions.[28] The recovery of RuO_2 guarantees a sustainable consumption of F radicals. HF, one product of the hydrolysis of ruthenium fluorides, can further react with Li^+ ions in the electrolyte as the reaction (5) to have LiF precipitated because the solubility of LiF in EC/DMC electrolytes should be very low, as the existence of LiF in SEI layers has been widely realized.[12] The more F radicals consumed, the less -CF_2O- groups formed and the more LiF precipitated. Accordingly, the RuO_2-4.5V has almost no -CF_2O- group and shows higher content of LiF in the range of sputtering for 30-90 s in comparison with the bare-4.5V, as shown in Fig. 4e. On the other hand, it is well known RuO_2 is an excellent catalyst for the electrochemical oxygen evolution. This catalytic ability probably accelerates oxygen evolution-involving reaction (6), an overall reaction of the (1-5), meanwhile, favours the consumption of F radicals and the formation of LiF.

$$xF^{\bullet} + RuO_2 \rightarrow RuF_x + O_2, \quad 4 \le x \le 6 \tag{2}$$

$$2RuF_x + xH_2O \rightarrow 2RuO_{x/2} + 2xHF \tag{3}$$

$$4RuO_{x/2} \rightarrow 4RuO_2 + (x-4)O_2 \tag{4}$$

$$HF + Li^+ \rightarrow LiF + H^+ \tag{5}$$

$$LiPF_6 + 2H_2O - 4e^- \xrightarrow{RuO2} PF_5 + LiF + 4H^+ + O_2 \tag{6}$$

Different from the case of RuO_2, the consumption amount of F radicals with Al_2O_3 by the reaction (7) is limited because the AlF_3 product is neither soluble in carbonate-based electrolytes nor hydrolysable.[55] The formation of AlF_3 on the surface of Al_2O_3 can completely hinders the sustainable consumption. In addition, Al_2O_3 has no catalytic activity for the electrochemical oxygen evolution. The reaction (8), an overall reaction of the (1) and (7), proceeds much slower than the reaction (6). Therefore, in the case of the Al_2O_3, the consumption of F radicals happens, but is limited and in a slower way. This consumption feature causes that the Al_2O_3-4.5V has less -CF_2O- groups than the bare-4.5V but more than the RuO_2-4.5V in the range of sputtering for 30-90 s, as shown in Fig. 3d. Because the reaction (8) does not involve the formation of LiF, the content of LiF in the SEI layer of the Al_2O_3-4.5V is close to that of the bare-4.5V, as shown in Fig. 4e.

$$12F^{\bullet} + 2Al_2O_3 \rightarrow 4AlF_3 + 3O_2 \tag{7}$$

$$12LiPF_6 - 12e^- + 2Al_2O_3 \rightarrow 12PF_5 + 4AlF_3 + 3O_2 + 12Li^+ \tag{8}$$

The amount of F radicals survived determines not only the content of -CF_2O- group, but also the length of the PEC chains. Fig. 5b shows how the length is affected. The more F radicals, the more EC molecular opened and the more short chains with a radical at one end formed. Two short chains can combine each other through forming bond between their radicals.[56] The combination chances become higher when the concentration of short chains is high. Therefore, the more F radicals are survived at the beginning, the shorter the PEC chains groups finally are formed with higher content of -CF_2O- groups, and vice versa, as shown in Fig. 5b. According to this analysis, among the three electrodes, the RuO_2-4.5V should have the longest PEC chains and the bare-4.5V has the shortest. The variation tendencies of the -CF_2O- content with sputtering (Fig. 3d) for the three electrodes support this analysis because with similar molecular structure, shorter polymer chains should be easier sputtered out than long ones.

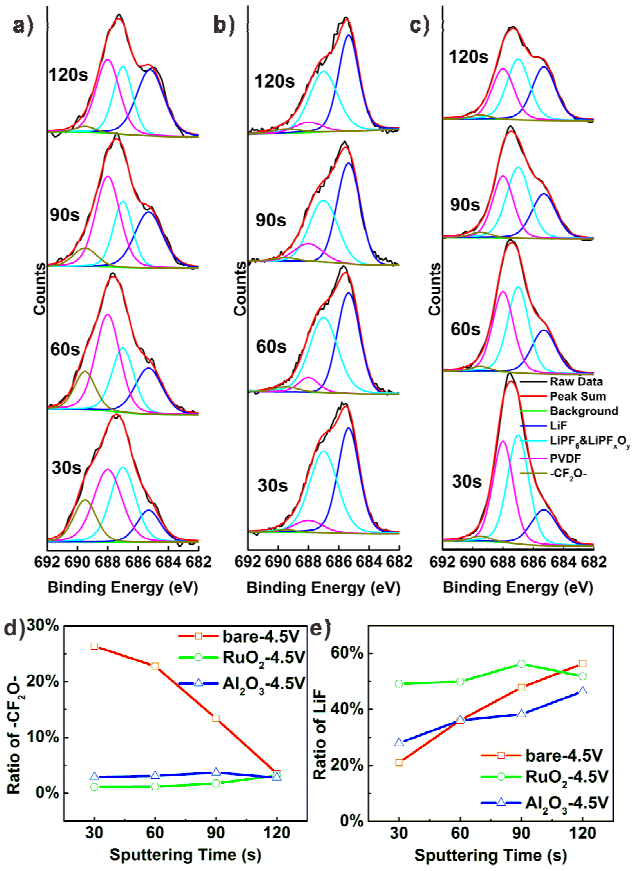

Fig. 4 F1s XPS of a) bare-4.5V, b) RuO_2-4.5V, c) Al_2O_3-4.5V after 500 cycles and Ar ion sputtering with 30, 60, 90 and 120 s. Variation of two area ratios with sputtering, d) the ratio of the F1s peak at 689.5 eV (-CF_2O-) and e) the ratio of F1s peak at 685.3 eV (LiF), respectively, with the sum of other F1s peaks except PVDF.

The length of the PEC chains also affects the variation of LiF content with sputtering. Because of faster etching of short PEC chains than LiF, the detected content of LiF for the bare-4.5V and Al_2O_3-4.5V increases with sputtering, as shown in Fig. 3e. The PEC chains for the Al_2O_3-4.5V should be shorter than that for the bare-4.5V, as the Al_2O_3 coated can consumes F radicals though limited. Therefore, we can note by a careful comparison that the increasing rate of LiF with sputtering for the Al_2O_3-4.5V is lower than that of the bare-4.5V. The content of LiF for the RuO_2-4.5V changes less with sputtering probably because of similar etching rate of the precipitated LiF with the long PEC chains and the uniform distribution of each component in its SEI layer in nano scale. For the same reason by the effect of the PEC chain length, the ratios between the metal-oxygen (M-O) O1s peak around 530 eV and the sum of other O1s peaks increase fastest with

sputtering for the bare-4.5V and slowest for the RuO_2-4.5V, as shown in Fig. S5d. The difference in etching rates for the PEC

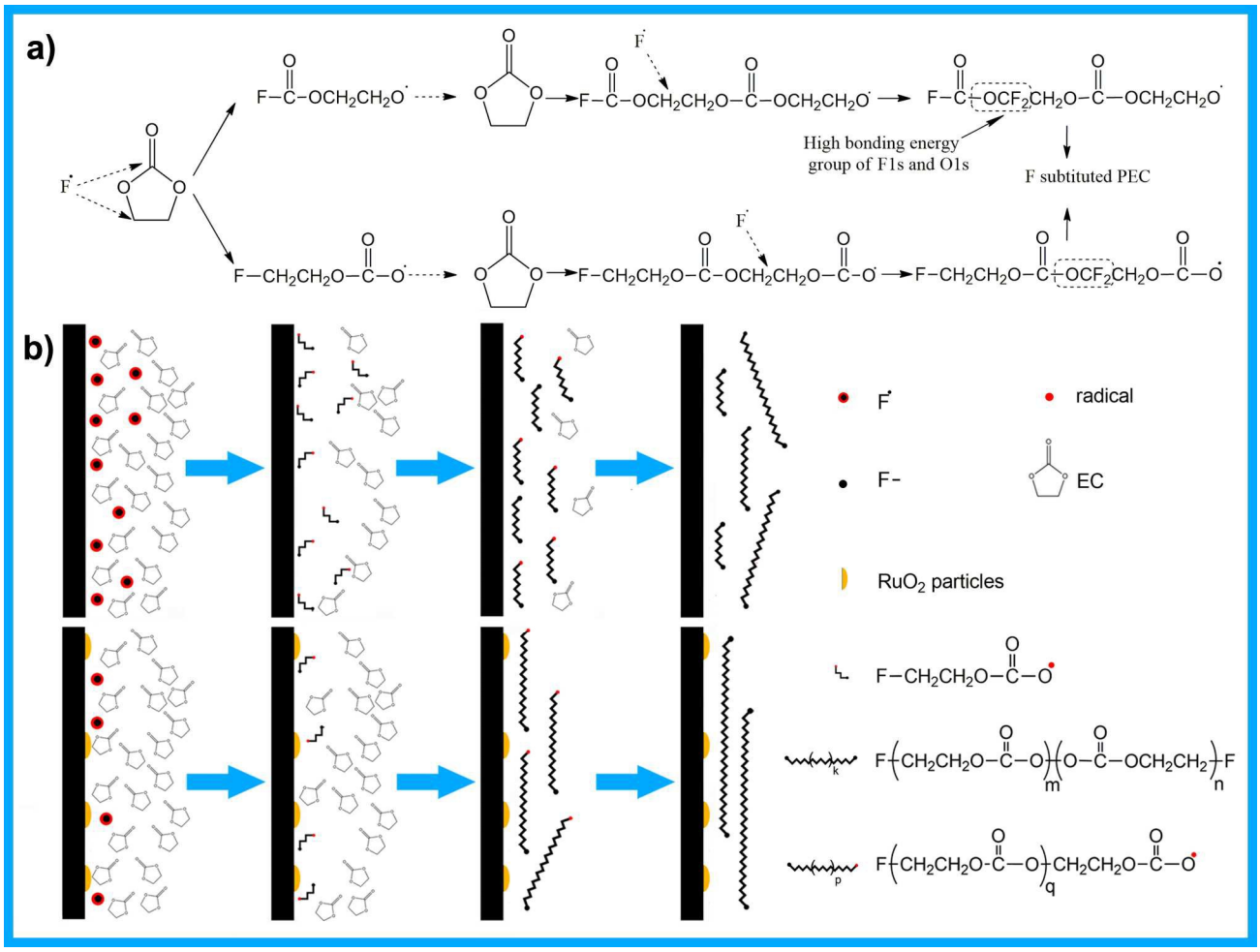

Fig. 5 a) Proposed reactions between F radicals and EC molecules, b) sketch map for the effect of F radical concentration on the length of F-substituted poly(ethylenecarbonate) chains.

chains with different lengths could also attribute to the close contents of the -CF_2O- group and LiF for the three electrodes after sputtering for 120 s.

In summary, the hydrolytic property of ruthenium fluorides, intermediate products during the formation of SEI layer on the RuO_2-4.5V, and the high catalytic activity of RuO_2 itself for electrochemical oxygen evolution can guarantee a sustainable consumption of the F radicals. This is crucial for the formation of the stable SEI layer. The AlF_3, product of the reaction of Al_2O_3 coated with F radicals, is neither soluble in carbonate-based electrolytes nor hydrolysable, and Al_2O_3 has no catalytic activity for the electrochemical oxygen evolution, leading to the formation of the unstable SEI layer. The stable SEI layer of the RuO_2-4.5V has the characteristic of longer PEC chains with extremely low content of -CF_2O- groups and relatively higher content of LiF. The distribution of the long PEC chains and LiF in its SEI layer is probably very uniform in nano scale. We consider these microstructural features are able to prevent the PF_6^- anions of the electrolyte from diffusing through the SEI layer to enter the high-potential region at the interface of LNMO with SEI layer. Accordingly, the formation of F radicals by the reaction (1) is hindered once a stable SEI layer is formed during beginning cycles, thus prevent the SEI layer from thickening in following cycles. The unstable SEI layers of the bare-4.5V and Al_2O_3-4.5V has the characteristic of short PEC chains with relatively higher content of -CF_2O- groups and lower content of LiF. The PF_6^- anions are easy to diffuse through this 'loose' SEI layers with short PEC chains to reach the high-potential region to keep forming F radicals, opening EC molecule ring and further initiating the polymerization.

Further improvement after optimizing the preparation of RuO_2-modified LNMO

A comparison between Fig. 1c-d and Fig. 6a-b clearly demonstrates that, if an 0.3 M LiOH solution was used instead of the NaOH solution to prepare RuO_2-modifed LNMO particles, the distribution uniformity of discrete RuO_2 particles on the surface of LNMO is improved greatly. Some large RuO_2 aggregates in micron scale are present among RuO_2-modifed

LNMO particles prepared with the NaOH solution (above-denoted as RuO_2-LNMO), while absent among the particles prepared with the LiOH solution (denoted as LiOH-RuO_2-LNMO), as shown in Fig S1a and Fig. S6. Accordingly, the coverage rate of RuO_2 on the LiOH-RuO_2-LNMO is higher than that on the RuO_2-LNMO. Fig. 6c illustrates that improving the distribution uniformity of RuO_2 particles leads to a further enhancement of cycle performance. The specific capacity of the LiOH-RuO_2-LNMO electrode discharged to 4.5 V is as high as 113.8 mAh/g after 1000 cycles.

Differences between charge and discharge medium potentials (potentials at half charge or discharge capacity, see Fig. S7) can reflect the extent of polarizations. The bigger differences mean the higher polarizations. Fig. 6d demonstrates the variations of the differences with cycling for the studied electrodes are consistent with their cycle performances. Among the all electrodes compared, the differences of the LiOH-RuO_2-LNMO electrode are lowest and increase with cycling in a lowest rate. This result proves that the LiOH-RuO_2-LNMO electrode has most stable SEI layer. The desirable cycle performance of the LiOH-RuO_2-LNMO does benefit from its higher coverage rate of RuO_2, which can favour a faster sustainable consumption of F fabrics and the formation of a more stable SEI layer in comparison with the RuO_2-LNMO electrode (RuO_2-4.5V). The cycle performance is also improved greatly by a modification with low-content RuO_2, such as only 0.5 wt%, as shown in Fig. S8. Considering the high cost of RuO_2 and the fact that the more RuO_2 deposited, the lower capacity of whole electrode, this result is worthwhile. Furthermore, the rate capability of LiOH-RuO_2-LNMO electrode is better than the bare electrode (Fig. S9) due to the electronic conductive nature of RuO_2.

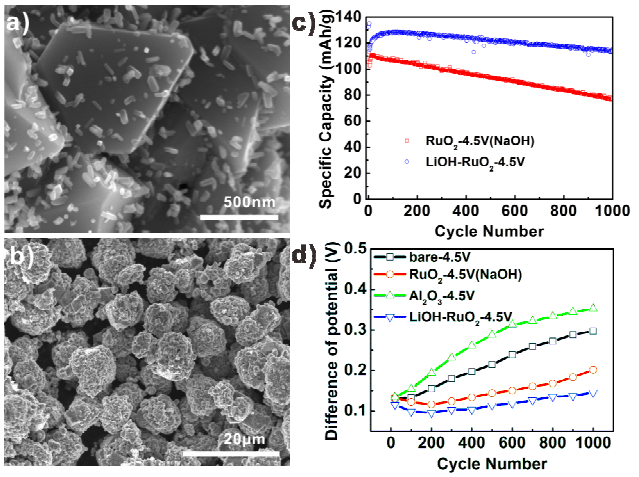

Fig. 6 a) and b) SEM images of the LiOH-RuO_2-LNMO prepared with the LiOH solution, c) cycle performance comparison between the LiOH-RuO_2-LNMO electrode with 4.5 V discharge cut-off potential and the RuO_2-4.5V (prepared with the NaOH solution), d) comparison of differences between charge and discharge medium potentials for the electrodes.

Conclusions

The cycle performance of LNMO is improved greatly by the surface modification with discrete RuO_2 particles in combination with setting discharge cut-off potential above the Mn^{3+}/Mn^{4+} plateau. The comparison among the Nyquist plots and SEI layers of the bare-4.5V, Al_2O_3-4.5V and RuO_2-4.5V indicates that a stable SEI layer of LNMO electrode should has the characteristic of relatively higher content of LiF and longer PEC chains with extremely low content of -CF_2O- groups. The crucial point for the formation of the stable SEI layer is a sustainable consumption of the F radicals generated by the electrochemical decomposition of $LiPF_6$ at high potentials. We consider that the sustainable consumption of the F radicals by the RuO_2 coated is dependent on the hydrolysable property of ruthenium fluorides, intermediate products during the formation of SEI layer on the RuO_2-4.5V, and the high catalytic activity of RuO_2 itself for electrochemical oxygen evolution. While the Al_2O_3 coated fails to attain the sustainable consumption because the product of the reaction of coated Al_2O_3 with F radicals, AlF_3, is inert. These differences concerned the chemical properties of RuO_2 and Al_2O_3 finally lead to the remarkable disparity between the RuO_2-4.5V and Al_2O_3-4.5V.

Acknowledgements

We acknowledge the financial support by NSFC (Grant No. 50872026 and 51272051), the Program for NCET and the Ph.D. Programs Foundation of Ministry of Education of China (Grant No. 20112302110014), Academic Expert Program of Harbin (RC2012XK017008). The authors also thank Dr. J.M. Shen of Northwestern University for the discussion about organic chemistry.

Notes and references

[a] *School of Materials Science and Engineering, Harbin Institute of Technology, Harbin, China. Fax: 86-451-86413922; Tel: 86-451-86413921; E-mail: htfang@hit.edu.cn*
[b] *School of electrical engineering and automation, Harbin Institute of Technology, Harbin, China.*
[c] *Canadian Light Source Inc., Saskatoon, Canada.*
† Electronic Supplementary Information (ESI) available: Fig. S1-S7. See DOI: 10.1039/b000000x/

1. A. Manthiram, K. Chemelewski and E. S. Lee, *Energy & Environmental Science*, 2014, **7**, 1339-1350.
2. A. Kraytsberg and Y. Ein-Eli, *Advanced Energy Materials*, 2012, **2**, 922-939.
3. S. Patoux, L. Daniel, C. Bourbon, H. Lignier, C. Pagano, F. Le Cras, S. Jouanneau and S. Martinet, *Journal of Power Sources*, 2009, **189**, 344-352.
4. J. Xiao, X. L. Chen, P. V. Sushko, M. L. Sushko, L. Kovarik, J. J. Feng, Z. Q. Deng, J. M. Zheng, G. L. Graff, Z. M. Nie, D. W. Choi, J. Liu, J. G. Zhang and M. S. Whittingham, *Advanced Materials*, 2012, **24**, 2109-2116.
5. M. G. Lazarraga, L. Pascual, H. Gadjov, D. Kovacheva, K. Petrov, J. M. Amarilla, R. M. Rojas, M. A. Martin-Luengo and J. M. Rojo, *Journal of Materials Chemistry*, 2004, **14**, 1640-1647.
6. H. B. Kang, S. T. Myung, K. Amine, S. M. Lee and Y. K. Sun, *Journal of Power Sources*, 2010, **195**, 2023-2028.

7. R. Singhal, M. S. Tomar, J. G. Burgos and R. S. Katiyar, *Journal of Power Sources*, 2008, **183**, 334-338.
8. Y. K. Sun, K. J. Hong, J. Prakash and K. Amine, *Electrochemistry Communications*, 2002, **4**, 344-348.
9. D. L. Liu, Y. Bai, S. Zhao and W. F. Zhang, *Journal of Power Sources*, 2012, **219**, 333-338.
10. T. Y. Yang, N. Q. Zhang, Y. Lang and K. N. Sun, *Electrochimica Acta*, 2011, **56**, 4058-4064.
11. Y. K. Fan, J. M. Wang, Z. Tang, W. C. He and J. Q. Zhang, *Electrochimica Acta*, 2007, **52**, 3870-3875.
12. J. Liu and A. Manthiram, *Chemistry of Materials*, 2009, **21**, 1695-1707.
13. H. M. Wu, I. Belharouak, A. Abouimrane, Y. K. Sun and K. Amine, *Journal of Power Sources*, 2010, **195**, 2909-2913.
14. J. C. Arrebola, A. Caballero, L. Hernan and J. Morales, *Journal of Power Sources*, 2010, **195**, 4278-4284.
15. K.-S. Lee, S.-T. Myung, K. Amine, H. YashiroB and Y.-K. Sun, *Journal of Materials Chemistry*, 2009, **19**, 1995-2005.
16. Z. H. Chen, D. J. Lee, Y. K. Sun and K. Amine, *Mrs Bulletin*, 2011, **36**, 498-505.
17. S. T. Myung, K. Amine and Y. K. Sun, *Journal of Materials Chemistry*, 2010, **20**, 7074-7095.
18. M. Thomas, P. G. Bruce and J. B. Goodenough, *Journal of the Electrochemical Society*, 1985, **132**, 1521-1528.
19. K. Xu and A. von Cresce, *Journal of Materials Chemistry*, 2011, **21**, 9849-9864.
20. J. B. Goodenough and Y. Kim, *Chemistry of Materials*, 2010, **22**, 587-603.
21. J. Liu and A. Manthiram, *Journal of the Electrochemical Society*, 2009, **156**, S13-S13.
22. Y. Kim, N. J. Dudney, M. Chi, S. K. Martha, J. Nanda, G. M. Veith and C. Liang, *Journal of the Electrochemical Society*, 2013, **160**, A3113-A3125.
23. X. Fang, M. Y. Ge, J. P. Rong and C. W. Zhou, *Journal of Materials Chemistry A*, 2013, **1**, 4083-4088.
24. J. Y. Shi, C. W. Yi and K. Kim, *Journal of Power Sources*, 2010, **195**, 6860-6866.
25. J. G. Li, Y. Y. Zhang, J. J. Li, L. Wang, X. M. He and J. Gao, *Ionics*, 2011, **17**, 671-675.
26. T. Noguchi, I. Yamazaki, T. Numata and M. Shirakata, *Journal of Power Sources*, 2007, **174**, 359-365.
27. L. Baggetto, N. J. Dudney and G. M. Veith, *Electrochimica Acta*, 2013, **90**, 135-147.
28. H. Over, *Chemical Reviews*, 2012, **112**, 3356-3426.
29. Y. G. Guo, Y. S. Hu, W. Sigle and J. Maier, *Advanced Materials*, 2007, **19**, 2087-+.
30. Y. S. Hu, Y. G. Guo, R. Dominko, M. Gaberscek, J. Jamnik and J. Maier, *Advanced Materials*, 2007, **19**, 1963-+.
31. J. Liu and A. Manthiram, *Journal of Materials Chemistry*, 2010, **20**, 3961-3967.
32. X. J. Yang, T. Yang, S. S. Liang, X. Wu and H. P. Zhang, *Journal of Materials Chemistry A*, 2014, **2**, 10359-10364.
33. J. H. Kim, S. T. Myung, C. S. Yoon, S. G. Kang and Y. K. Sun, *Chemistry of Materials*, 2004, **16**, 906-914.
34. S. F. Yang, J. Chen, Y. J. Liu and B. L. Yi, *Journal of Materials Chemistry A*, 2014, **2**, 9322-9330.
35. H. Duncan, B. Hai, M. Leskes, C. P. Grey and G. Y. Chen, *Chemistry of Materials*, 2014, **26**, 5374-5382.
36. S. T. Myung, K. S. Lee, D. W. Kim, B. Scrosati and Y. K. Sun, *Energy & Environmental Science*, 2011, **4**, 935-939.
37. Y. Y. Xia, Y. H. Zhou and M. Yoshio, *Journal of the Electrochemical Society*, 1997, **144**, 2593-2600.
38. K. Amine, H. Tukamoto, H. Yasuda and Y. Fujita, *Journal of the Electrochemical Society*, 1996, **143**, 1607-1613.
39. B. Z. Li, L. D. Xing, M. Q. Xu, H. B. Lin and W. S. Li, *Electrochemistry Communications*, 2013, **34**, 48-51.
40. M. Matsui, K. Dokko and K. Kanamura, *Journal of the Electrochemical Society*, 2010, **157**, A121-A129.
41. M. D. Levi and D. Aurbach, *Journal of Physical Chemistry B*, 2004, **108**, 11693-11703.
42. R. Alcantara, M. Jaraba, P. Lavela and J. L. Tirado, *Journal of Electroanalytical Chemistry*, 2004, **566**, 187-192.
43. M. H. Ryou, G. B. Han, Y. M. Lee, J. N. Lee, D. J. Lee, Y. O. Yoon and J. K. Park, *Electrochimica Acta*, 2010, **55**, 2073-2077.
44. H. Duncan, Y. Abu-Lebdeh and I. J. Davidson, *Journal of the Electrochemical Society*, 2010, **157**, A528-A535.
45. S. Y. Bae, W. K. Shin and D. W. Kim, *Electrochimica Acta*, 2014, **125**, 497-502.
46. H. Sclar, O. Haik, T. Menachem, J. Grinblat, N. Leifer, A. Meitav, S. Luski and D. Aurbach, *Journal of the Electrochemical Society*, 2012, **159**, A228-A237.
47. B. Ziv, V. Borgel, D. Aurbach, J. H. Kim, X. C. Xiao and B. R. Powell, *Journal of the Electrochemical Society*, 2014, **161**, A1672-A1680.
48. L. Yang, B. Ravdel and B. L. Lucht, *Electrochemical and Solid State Letters*, 2010, **13**, A95-A97.
49. S. Dalavi, M. Xu, B. Knight and B. L. Lucht, *Electrochemical and Solid State Letters*, 2012, **15**, A28-A31.
50. D. Bar-Tow, E. Peled and L. Burstein, *Journal of the Electrochemical Society*, 1999, **146**, 824-832.
51. V. R. Koch, L. A. Dominey, C. Nanjundiah and M. J. Ondrechen, *Journal of the Electrochemical Society*, 1996, **143**, 798-803.
52. S. E. Sloop, J. B. Kerr and K. Kinoshita, *Journal of Power Sources*, 2003, **119**, 330-337.
53. I. A. Shkrob, Y. Zhu, T. W. Marin and D. Abraham, *Journal of Physical Chemistry C*, 2013, **117**, 19255-19269.
54. Greenwood, *Chemistry of Elements*, 1998.
55. S. T. Myung, K. S. Lee, C. S. Yoon, Y. K. Sun, K. Amine and H. Yashiro, *Journal of Physical Chemistry C*, 2010, **114**, 4710-4718.
56. G. M. D. H. Solomon, *THE CHEMISTRY OF RADICAL POLYMERIZATION*, 2006.

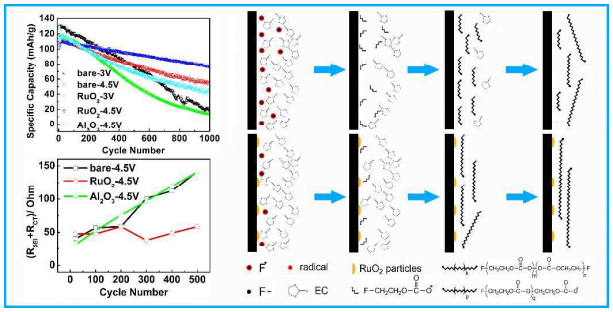

RuO_2 particles on $LiNi_{0.5}Mn_{1.5}O_4$ sustainably consume the F radicals leading to the formation of a stable SEI layer, which is the reason for improving the cycle performance by the surface modification with the discrete RuO_2 particles in combination with setting discharge cut-off potentials to 4.5 V.